

PCCP

Accepted Manuscript



This is an *Accepted Manuscript*, which has been through the Royal Society of Chemistry peer review process and has been accepted for publication.

Accepted Manuscripts are published online shortly after acceptance, before technical editing, formatting and proof reading. Using this free service, authors can make their results available to the community, in citable form, before we publish the edited article. We will replace this *Accepted Manuscript* with the edited and formatted *Advance Article* as soon as it is available.

You can find more information about *Accepted Manuscripts* in the [Information for Authors](#).

Please note that technical editing may introduce minor changes to the text and/or graphics, which may alter content. The journal's standard [Terms & Conditions](#) and the [Ethical guidelines](#) still apply. In no event shall the Royal Society of Chemistry be held responsible for any errors or omissions in this *Accepted Manuscript* or any consequences arising from the use of any information it contains.

Electronic structure of para-benzoquinone radical anion revisited

Alexander A. Kunitsa^{a,b} and Ksenia B. Bravaya^a

^aDepartment of Chemistry, Boston University, Boston, Massachusetts, 02215

^bInstitute of Problems of Chemical Physics, Chernogolovka, Russia, 142432

Photoinduced dynamics in para-benzoquinone anion features a subtle interplay between autodetachment and non-adiabatic transitions involving a dense manifold of resonances. We report the results of multistate multireference perturbation theory study of the electronic structure of the para-benzoquinone anion in the ground, several low-lying excited electronic states, and in the lowest electron-detached state (the ground state of the neutral molecule). The electronic structure calculations revealed non-planar equilibrium geometry of the 2A_u excited state of the anion, but the effects of non-planarity on the shape of the absorption spectrum are found to be minor. Despite the large differences in the vertical excitation energies for the two lowest bright excited states, 2A_u (2.55 eV) and ${}^2B_{3u}$ (2.93 eV), the simulated absorption spectra overlap significantly for the photon energies below 2.7 eV. Relevant minimum energy conical intersection points have been located using the CASSCF method. Excited-state deactivation channels are discussed in the context of the accurate energetics and recent spectroscopic studies of the para-benzoquinone anion.

I. INTRODUCTION

Unique electron accepting properties of quinones make them integral components of molecular assemblies involved in biological electron transfer [1–5]. Electron attachment to quinones is a thermodynamically favorable process leading to stable charge separation at intermediate steps of photosynthesis [3, 4] and cellular respiration [5]. Such highly exothermic reactions often fall into the inverted Marcus region and proceed with low rate constants [6]. Yet, electron attachment to several quinones in non-polar solvents exhibits marked deviations from the Marcus theory behavior [7, 8] and occurs on the time-scales of nearly barrierless reactions. The reported high values of the apparent rate constants were initially attributed to the formation of the electronically excited anions [7]. The fundamental insights into the mechanisms of electron capture by quinones were obtained from the experimental studies of p-benzoquinone

(pBQ) [8–11], the simplest quinone model system. Temperature [8] and pressure dependence [10] of the electron capture rates to pBQ in various non-polar solvents was rationalized by an initial electron capture to the $\pi\pi^*$ excited state of the anion and subsequent relaxation to the ground state via the manifold of the dark $n\pi^*$ states, which occurs on the nanosecond timescale [9]. The detailed information on the nature of these states had been extracted from the gas phase studies of pBQ \bullet^- [13–19]. Although pBQ itself has a positive electron affinity, the lowest bright excited states of the isolated molecular anion are metastable with respect to electron detachment and have finite lifetimes [13, 14, 20].

The electronic structure of metastable anions in the gas phase can be probed in either full-collision or half-collision experiments [21]. The former group of techniques relies on the scattering characteristics of incident electrons by neutral molecules while the latter deals with the autodetachment of transient anions initially prepared in metastable resonance states [22, 23]. The two groups provide complementary information as they allow one to probe autodetachment at different molecular geometries - the equilibrium geometry of the neutral parent molecule and the corresponding anion, respectively. Both approaches were applied to pBQ \bullet^- . The key processes initiated by photoexcitation of pBQ \bullet^- are illustrated in Fig. 1. Electron attachment to neutral pBQ can, in turn, proceed either directly to the ground electronic state of the anion or via excited metastable electronic states followed by the relaxation to the ground electronic state.

Metastable states of isolated anionic pBQ were first observed by Christophorou et al. [18]. The resonance was located at 2.1 eV above the ground state of the neutral [17, 18]. Further cesium collision ionization mass-spectrometry, electron transmission, and electron energy loss spectroscopy studies revealed several low-lying resonances at 0.7, 1.4, and 1.9-2.1 eV [15, 16]. The resonances were assigned to the excited states of pBQ \bullet^- [15]. Importantly, the decay of the resonances at 1.4 eV [15] and 2.1 eV [16] exhibited a two-channel behavior, with the slow components in the pico- to nanosecond range. The long lifetimes of the metastable anion states have been rationalized by proposing the initial formation of the excited state of the anion followed by fast relaxation to the long-lived ground electronic state, which can proceed either directly or via intermediate excited electronic states.

Thorough photoelectron photodetachment spectroscopy studies of pBQ \bullet^- by Schiedt and Weinkauff [20] indeed demonstrated the existence of multiple resonances at 2.1-2.5 eV above the ground state of the anion. The resonance features were assigned to 2A_u shape resonance,

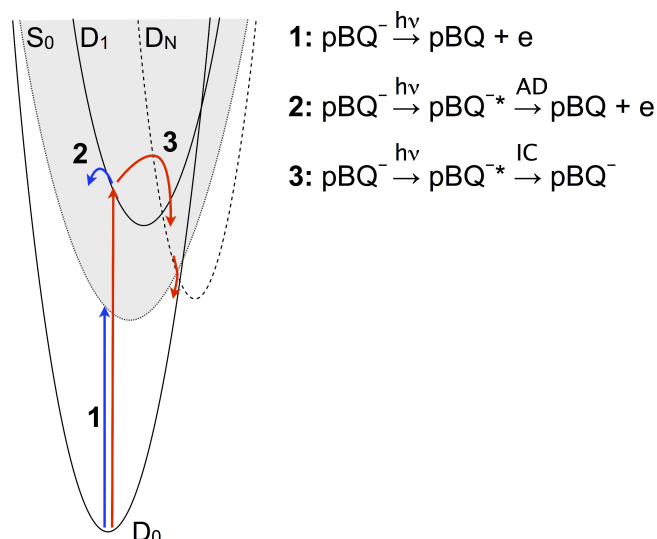


FIG. 1: Possible photoinduced processes in the pBQ anion: direct photodetachment (1), resonant excitation followed by autodetachment, AD, (2), and resonant excitation followed by radiationless relaxation back to the ground electronic state via internal conversion, IC, (3). Potential energy curves of the ground and bright excited states (solid), dark electronic states (dashed), and the ground electronic state of the neutral molecule (dotted) are shown.

and one or two Feshbach resonances, presumably of the B_{2u} and B_{3g} symmetry. The shape and Feshbach resonances in this case correspond to optically bright and dark states, respectively. The assignment is supported by the results of the CASPT2 and SAC-CI calculations that place the 2A_u state at 2.82 [24] and 2.71 [25] eV, respectively. Electronic structure calculations also consistently identify another bright excited state of the ${}^2B_{3u}$ symmetry lying slightly higher in energy (2.8 - 3.5 eV [14, 24, 25]). The energy range of 2.5 - 3.1 eV has been explored recently by Verlet and co-authors [13, 14]. Photoinduced dynamics at 3.1 eV has been probed by time-resolved photoelectron spectroscopy [14]. The results pointed to rapid interconversion between the bright ${}^2B_{3u}$ and 2A_u states of $\text{pBQ}^{\bullet-}$ on the timescale of ≈ 20 fs. Based on the time-resolved photoelectron spectroscopy data and the proposed kinetic model the authors estimated the lifetimes of the ${}^2B_{3u}$ and 2A_u states to be less than 30 fs and 27 fs, respectively [14].

The interplay between electron detachment and relaxation processes inherent to $\text{pBQ}^{\bullet-}$, had been further analyzed with frequency-resolved and angular-resolved photoelectron imaging [13], which revealed the abrupt change of photoelectron angular distribution (PAD) in the 2.5-3.1 excitation energy range. Specifically, PAD exhibited parallel polarization at 2.5 - 2.7 eV

but became isotropic at 2.7-3.1 eV, which was explained by dominant population of the 2A_u state at energies below 2.7 eV, and excitation into ${}^2B_{3u}$ above 2.7 eV. Yet, there are multiple examples where the PAD anisotropy parameter changes dramatically with excitation energy when passing single resonance [26, 27]. Thus, the experimental studies of the photoinduced processes in $\text{pBQ}^{\bullet-}$ in the 2.1 - 3.1 energy range point to an entangled dynamics involving multiple internal conversion and autodetachment pathways with the major players being the two bright excited states, 2A_u and ${}^2B_{3u}$, several dark excited states of the $n\pi^*$ type, and the ground state of the neutral. Recently, it was shown that photoinduced dynamics in coenzyme- Q_0 , the chemical analogue of $\text{pBQ}^{\bullet-}$, can be also rationalized taking into account two bright states correlating with 2A_u and ${}^2B_{3u}$, which suggests a universal nature of relaxation processes in $\text{pBQ}^{\bullet-}$ [28].

From the theoretical standpoint, the interpretation of the experimental data for $\text{pBQ}^{\bullet-}$ poses several challenges. First, the low-lying electronic states of $\text{pBQ}^{\bullet-}$ are vertically unbound with respect to electron loss [13, 14, 24, 25] and, thus, are electronic resonances rather than true stationary states. The rigorous account of their non-stationary character requires special theoretical tools, e.g. complex scaling [21, 29, 30] or complex absorbing potential (CAP) [31–34] methods, and is beyond the scope of the present work. Second, the experimental data suggests that the non-adiabatic transitions play a role in the relaxation dynamics. Therefore, it is essential to accurately describe the relative energies of the $\text{pBQ}^{\bullet-}$ electronic states in the vicinity of their degeneracy manifolds where the static correlation effects can be strong. This problem can be addressed, for example, with multi-reference electronic structure methods, and in particular with different flavors of multistate multireference perturbation theory. The latter approach was adopted in the most recent study by West *et al.* [13]. The manifold of low-lying $\text{pBQ}^{\bullet-}$ electronic states identified in their extended multiconfigurational quasidegenerate perturbation theory (XMCQDPT2) calculations differs from the previous complete active space second order perturbation theory (CASPT2, [35]) results [14, 24]. This discrepancy might be due the appearance of additional mixed valence-diffuse state of ${}^2B_{3u}$ symmetry, as mentioned in Ref. [28].

Here we present the results of electronic structure calculations of energetics, geometries, relevant conical intersection minimum energy points, and spectral features of the $\text{pBQ}^{\bullet-}$ anion. Specifically, we address the following questions.

- What states of $\text{pBQ}^{\bullet-}$ are populated upon excitation at 2.4 - 3.1 eV?

- What are the possible electron relaxation mechanisms for $\text{pBQ}^{\bullet-}$ excited within this energy range?

The manuscript is organized as follows. Section II summarizes the details of the computational approach. We report the computed vertical and adiabatic excitation energies of the $\text{pBQ}^{\bullet-}$ anion in Section III A. The equilibrium geometries of the two bright excited states (2A_u and ${}^2B_{3u}$) and the shape of the simulated absorption spectra are discussed in Sections III B and III C, respectively. The energies and geometries of relevant minimum energy crossing points (MECP) are summarized in Section III D. Finally, we analyze the direct and resonant photodetachment channels of $\text{pBQ}^{\bullet-}$ as well as its electronic relaxation pathways in 2.4 - 3.1 eV energy interval in Section III E.

II. COMPUTATIONAL DETAILS

Geometries of $\text{pBQ}^{\bullet-}$ in the ground and excited states were optimized with multireference Møller-Plesset perturbation theory of second order (MRMP2) [36] using corresponding complete active space self-consistent field (CASSCF) zero-order wave functions. Active space comprised eight π and four lone pair orbitals on oxygen atoms (SI, Section I). To verify whether the stationary points correspond the true minima, the harmonic frequencies were computed with CASSCF for the equilibrium geometries obtained at the same level. D_{2h} or D_2 symmetry was imposed depending on the type of target electronic state. Vertical energy gaps (excitation and detachment energies) were evaluated at each equilibrium geometry using XMCQDPT2 [37]. XMCQDPT2 is a multi-state multireference second order perturbation approach, which utilizes the construction and diagonalization of effective Hamiltonian on the multidimensional model space. It is known to provide accurate energy gaps (SI, Section II) and is well-behaved in the vicinity of quasi-degeneracy points of several electronic states [38, 39]. In our calculations the model space included ten zero-order CASSCF solutions with state-averaging over the ten states.

Transition dipole moments and oscillator strengths were computed using XMCQDPT2 wave functions, which are linear combinations of the CASSCF reference states mixed by perturbation. The corresponding Franck-Condon factors were evaluated in double-harmonic parallel normal mode approximation using the ezSpectrum software [40], unless stated otherwise. The effect of Duschinsky rotation on the simulated spectra was found to be negligible (SI, Section III).

MECP for the low-lying states were located using penalty function algorithm [41]. MECP search was performed at the CASSCF level with averaging over two target states. The resulting energies of the states at MECP were calculated with MRMP2 based on the CASSCF functions optimized separately for each of the degenerate states.

Intruder state avoidance technique [42] with level shift of 0.02 Hartree was used in all perturbation theory calculations throughout the work.

The cc-pVTZ basis was used for carbon and hydrogen atoms. In order to account for the diffuse character of electron density in pBQ \bullet^- , the basis set on the oxygen atoms was augmented by diffuse functions (d-aug-cc-pVTZ). The XMCQDPT2 and CASSCF calculations were carried out with the Firefly package [43]. Frequency analysis was performed with GAMESS(US) [44] with 6-311++G(2d,p) basis. The Q-Chem [45] software was used for equation-of-motion coupled-cluster electron attachment (EOM-EA-CCSD) calculations.

III. RESULTS AND DISCUSSION

A. Electronic structure of the p-benzoquinone radical anion

Photoinduced dynamics following pBQ \bullet^- excitation at 2.5 - 3.1 eV is governed by the metastable excited states of the anion and the lowest electron-detached state (Fig. 2). Several excited resonance states can be populated in this energy range: two bright $\pi\pi^*$ states (2A_u and $^2B_{3u}$) and a set of optically forbidden $n\pi^*$ and $\pi\pi^*$ states. This ladder of electronic states provides multiple radiationless relaxation pathways. Therefore, the information on relative energies of the states involved is essential for understanding the photophysics of pBQ \bullet^- .

XMCQDPT2 places the 2A_u and $^2B_{3u}$ states at 2.55 and 2.93 eV vertically above the $^2B_{2g}$ ground state. The next bright state ($(^2)^2B_{3u}$) is located at 4.25 eV and is well separated in energy. The oscillator strengths of the $^2A_u \leftarrow ^2B_{2g}$ and $^2B_{3u} \leftarrow ^2B_{2g}$ transitions are close (0.09 and 0.10, respectively). A set of the dark $n\pi^*$ states ($^2B_{2u}$, $^2B_{3g}$) lying below 2A_u and the optically forbidden $\pi\pi^*$ $^2B_{1g}$ state at 0.2 eV above $^2B_{3u}$ (Table I) have been located. The energetic proximity of the dark and bright states suggests that the former can play a role in radiationless relaxation.

The vertical detachment energy (VDE) of pBQ \bullet^- is 2.17 eV (Table I). Thus, all the states of interest except $^2B_{2u}$, which is weakly bound, are electronic resonances and can undergo decay

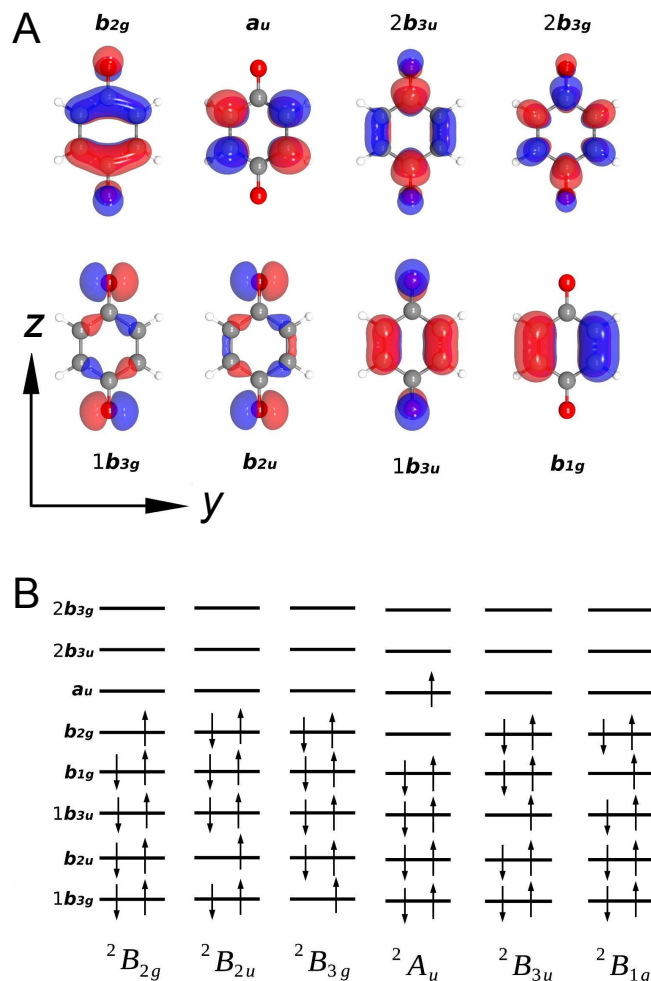


FIG. 2: Relevant active space molecular orbitals (A) and leading electronic configurations of the low-lying $\text{pBQ}^{\bullet-}$ states (B). The orientation of the coordinate system is shown in the left bottom corner of panel A.

to the ${}^1A_g + e$ autodetachment continuum of pBQ (Fig. 3). The states can be classified as shape or Feshbach resonances based on the analysis of their wave functions (Fig. 2). The 2A_u state is dominated by the $b_{2g} \rightarrow a_u$ excitation. It can decay through a one-electron transition to 1A_g state of the neutral and can, therefore, be classified as a shape resonance[21]. Our recent CAP/EOM-EA-CCSD calculation [34] showed that 2A_u lifetime is ≈ 51 fs. In contrast, the decay of other states is formally a two-particle process driven by electron correlation and is expected to be slower. Indeed, the peaks in the photodetachment cross section associated with the Feshbach resonances are much more narrow than the one attributed to the 2A_u shape resonance [20].

The electronic structure of electron-detached, ground, and excited states of $\text{pBQ}^{\bullet-}$ has been

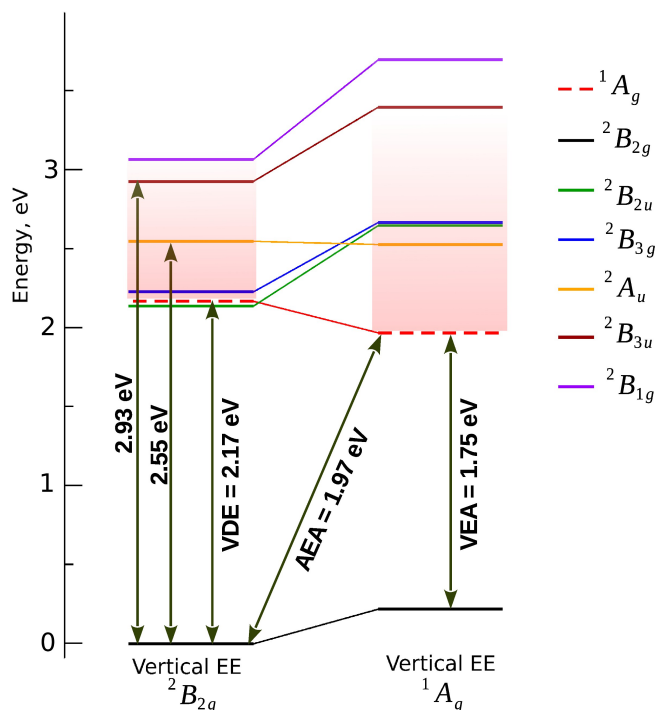


FIG. 3: Vertical ordering of the ground, excited, and electron-detached states of $\text{pBQ}^{\bullet-}$. Vertical energy gaps at the two equilibrium geometries are shown: for the ground state of the anion (${}^2B_{2g}$) and for the ground state of the neutral (1A_g). Shaded areas indicate the photodetachment continuum at the corresponding geometries.

extensively studied computationally [12, 14, 24, 25]. The SAC-CI SD-R method yields $\text{pBQ}^{\bullet-}$ excitation energies that tend to be higher [25] relative to our XMCQDPT2 values. Most notably, the SAC-CI results in ${}^2B_{2g} - {}^2B_{3u}$ and ${}^2B_{2g} - {}^2B_{1g}$ vertical energy gaps that are overestimated by 0.6 eV compared to the present results. CASPT2, which is conceptually similar to MRMP2, results in vertical energy gaps [24] similar to those reported here. Interestingly, ${}^2B_{3u}$ and 2A_u appear to be almost degenerate (the corresponding vertical excitation energies are 2.80 and 2.82 eV) at the CASPT2 level [24] compared with 0.38 eV energy difference obtained in our calculation. This discrepancy can be possibly explained by imbalanced description of the ${}^2B_{3u}$ and 2A_u states due to the extra b_{3u} orbital which was added to the active space to avoid intruder states problems. Horke *et al.* [14] reported vertical excitation energies to the ${}^2B_{3u}$ and 2A_u states of 3.13 eV and 2.58 eV, respectively. In this case, the active space was augmented by the two lone pair orbitals (10 active orbitals in comparison to 8 π orbitals in CASPT2 calculations [24]) and the IPEA correction [46] was applied. The major differences between the two CASPT2 studies could be due to the IPEA correction which is known to yield ~ 0.2

TABLE I: Vertical energy gaps (eV) for pBQ \bullet^- computed at its ground state equilibrium geometry (${}^2B_{2g}$) and at the equilibrium geometry of the neutral (1A_g).

State	XMCQDPT2/ SA(10)-CASSCF(17,12)		XMCQDPT2/ CASSCF(17,12) [14]		Electron scattering resonances [16]
	Geometry ${}^2B_{2g}$	1A_g	${}^2B_{2g}$	1A_g	
${}^2B_{2g}$	0.00	-1.75	0.00	-1.63	
1A_g	2.17	0.00	1.98	0.00	
${}^2B_{2u}$	2.14	0.68	2.38	0.4	0.72
${}^2B_{3g}$	2.23	0.7	2.38	0.9	
2A_u	2.55	0.56	2.78	0.4	
(1) ${}^2B_{3u}$	2.93	1.43	2.98	0.7	1.43
${}^2B_{1g}$	3.07	1.73	–	–	
(2) ${}^2B_{3u}$	4.25	2.14	3.18	1.9	2.15
(3) ${}^2B_{3u}$	–	–	4.48	2.4	

eV energy shifts [47], although the effects of the extra lone pair orbitals cannot be completely ruled out. Recent electronic structure calculations of pBQ \bullet^- were performed by West *et al.* [13] at the XMCQDPT2/aug-cc-pVTZ-f level of theory (Table I). We note several differences between their estimates and the results reported here. West *et al.* identified the two ${}^2B_{3u}$ states in the interval of 2.9 - 3.2 eV. The first ${}^1{}^2B_{3u}$ state with energy 2.98 eV above ${}^2B_{2g}$ was reported to have negligible oscillator strength in their calculation. The second ${}^2B_{3u}$ state is optically allowed and has vertical excitation energy 3.18 eV. While the bright state has been identified by previous computational studies [14, 24, 25], the existence of the dark state is only supported by the SAC-CI results of Honda *et al.* [25]. It should be noted that at the SAC-CI level this state appears at 2.48 eV and has a pronounced pseudocontinuum character. The differences in the ordering and relative energies of pBQ \bullet^- electronic states are also noticeable at the equilibrium geometry of the neutral pBQ. In particular the authors assigned the first excited state as ${}^2B_{3u}$, whereas our calculations predict it to be the 2A_u state. Overall, all electronic structure calculations consistently put the two bright excited states, ${}^2B_{3u}$ and 2A_u , close in energy and reveal a manifold of dark excited states of anion within the 2.5-3.1 eV energy

range. At the same time, as discussed in Secs. III B and III C, several important structural and electronic aspects that affect interpretation of the experimental results have been overlooked.

Photoinduced electron detachment and electron capture by $\text{pBQ}^{\bullet-}$ have been subject to several gas phase spectroscopic studies [15–18, 20]. The energy dependence of the photodetachment cross section obtained by Schiedt and Weinkauff [20] was rationalized by postulating the existence of the one or two narrow $n\pi^*$ Feshbach resonances embedded in photodetachment continuum at energies 2.2 - 2.43 eV and a broad shape resonance at 2.5 eV which was assigned as the 2A_u state. Our calculations support this assignment. Computed adiabatic electron affinity of 1.97 eV is also in good agreement with the experimental value by Schiedt and Weinkauff (1.860 ± 0.005 eV) [20]. Electron transmission experiments conducted by Allan [16] revealed three short-lived states at 0.72, 1.43 and 2.15 eV above the ground state of neutral pBQ. Our analysis suggests that the first state could be assigned as 2A_u , whereas the other two are the ${}^2B_{3u}$ states (Table I). As mentioned earlier, the first ${}^2B_{3u}$ state exhibits a Feshbach resonance character and can have relatively long lifetime. Note that this state acquires significant shape character due to the increased contribution of the $b_{2g} \rightarrow 1b_{3u}$ excited configuration to its CASSCF wave function at the geometry of the neutral pBQ and, thus, might be responsible for the broad band at 1.43 eV observed in scattering experiments.

Presented vertical excitation energy calculations place the ${}^2B_{3u}$ excited state significantly above the 2A_u state and are consistent with the results of previous theoretical studies. At the same time, detailed understanding of the competing population of the 2A_u and ${}^2B_{3u}$ states requires information on the vibrationally-resolved cross-sections. Therefore, we start by discussing the equilibrium geometries of the bright excited states in Sec. III B and proceed to the analyzing the shape of the simulated vibronic absorption spectra in Sec. III C.

B. Equilibrium geometries of the bright states of $\text{pBQ}^{\bullet-}$

The pBQ radical anion is planar and has D_{2h} symmetry in the ground state. Anticipated geometry changes upon excitation can be deduced from the nodal structure of the molecular orbitals involved. The following discussion focuses on the equilibrium structures of $\text{pBQ}^{\bullet-}$ in two lowest bright states, 2A_u and ${}^2B_{3u}$, which are accessible at energies 2.5 - 3.1 eV. The 2A_u state can be described as the $b_{2g} \rightarrow a_u$ excitation from the ${}^2B_{2g}$ state. The a_u orbital has nodes on the double C-C bonds and is non-bonding over the C-(C=O)-C fragments of the carbon ring

leading to a partial sp^3 character of the carbon atoms once populated. This may result in the distortion of the ring driven by (a) pyramidalization and (b) weak bonding interaction of the carbon atoms on its opposite sides. Indeed, the unconstrained MRMP2 geometry optimization leads to a D_2 non-planar equilibrium structure with a D_{2h} saddle point (Fig. 4). The deviation from planarity measured by the C_OCCC_O dihedral angle, is 28.1° for the D_2 geometry. The corresponding relaxation energy is 0.17 eV (3.9 kcal/mol) at the MRMP2 level.

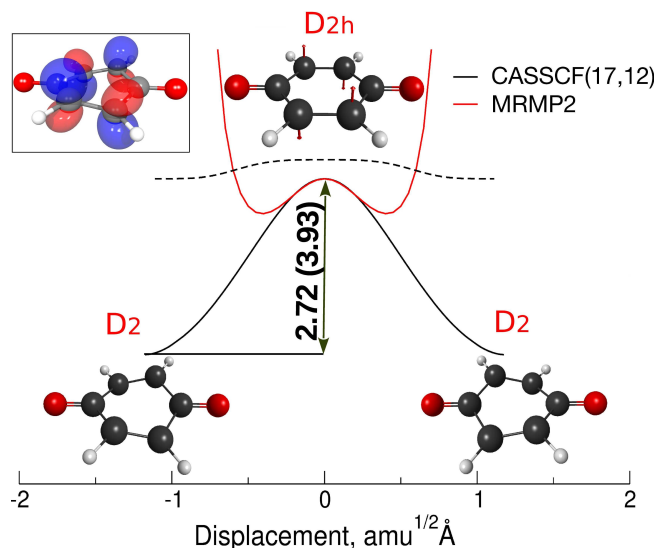


FIG. 4: Potential energy scans along the ($^2A_u(D_{2h}) \rightarrow A(D_2)$) twisting reaction coordinate. The CASSCF(17,12) IRC path is shown in black. CASSCF and MRMP2 (in parenthesis) transition-state energies are given in kcal/mol with respect to the D_2 equilibrium geometry of the A_u state. The red curve corresponds to the MRMP2 scan along the a_u mode with imaginary frequency of $335i \text{ cm}^{-1}$ at the planar TS D_{2h} geometry. The ground-state vibrational wave function for the corresponding one-dimensional potential is shown by the black dashed curve. The 2A state (D_2 symmetry) SOMO is shown in the inset.

The EOM-EA-CCSD calculations result in the relaxation energy of 0.15 eV, which is consistent with the MRMP2 value of 0.17 eV. The CASSCF(17,12)/6-311++G(2d,p) intrinsic reaction coordinate (IRC) path shows that the initial movement along the twisting coordinate is associated with the a_u normal mode with imaginary frequency $335i \text{ cm}^{-1}$ as shown in Fig. 4. This imaginary frequency normal mode was previously mentioned by Pou-Amerigo *et al.* [24], yet, the equilibrium geometry was not reported. Further relaxation occurs along the two a_g normal modes with frequencies 480 and 832 cm^{-1} suggesting that the twisting occurs in at least

three-dimensional normal mode space. The participation of additional higher frequency normal modes can account for relatively large D_{2h} to D_2 relaxation energy. Interestingly, this energy is large enough to make $A(D_2)$ state vertically bound by 0.05 eV although adiabatically it still belongs to autodetachment continuum lying 0.3 eV above the ground states of neutral pBQ. Overall geometry changes upon the ${}^2A_u \leftarrow {}^2B_{2g}$ excitation can be described as a combination of twisting, carbon ring expansion, and C-O bond contraction (SI, Section IV). The character of geometry changes for the second bright state ${}^2B_{3u}$ is qualitatively different: the equilibrium C-O bond length is longer compared to the ground ${}^2B_{2g}$ state, while the changes in the carbon ring are moderate. This is consistent with the shape of the $1b_{3u}$ orbital shown in Fig. 2.

C. Absorption spectrum of pBQ $^{\bullet-}$

The qualitative difference between 2A_u and ${}^2B_{3u}$ geometries is reflected in the Franck-Condon (FC) factors and the shape of the corresponding excitation bands. The complicated topography of the 2A_u potential energy surface in the Franck-Condon region makes the calculation of ${}^2A_u \leftarrow {}^2B_{2g}$ FC factors non-trivial due to the possible delocalization of the vibrational wave functions over the two potential minima corresponding to the D_2 structures. Moreover, several normal modes are coupled along the twisting path meaning that the coordinates in the nuclear vibrational problem cannot be separated. Here, we employ simple parallel normal mode approximation to gain an insight into the qualitative features of the gas-phase pBQ $^{\bullet-}$ absorption spectrum. The ${}^2A_u \leftarrow {}^2B_{2g}$ FC factors were calculated using two complementary approaches. In the first, D_{2h} geometry (the 2A_u state saddle point, Fig. 4) geometry was used and the FC factors were evaluated within the harmonic approximation for all normal modes except the twisting a_u mode. The vibrational problem for the a_u mode was solved numerically for the double-well potential obtained as a rigid MRMP2 surface scan along the mode (SI, Section V). This potential exhibits two shallow minima separated by the 0.4 kcal/mol barrier. The energy of its first vibrational level is 6.7×10^{-4} eV below the top of the barrier and the ground-state wave function is delocalized over the two wells (Fig. 4). The second energy level is 0.06 eV above the barrier. As the FC factors for the a_u mode tend to decrease quickly with level number in this approximation (0.886, 0.112 and 0.0026 for 0-0, 0-2 and 0-4 transitions), we neglected excitations with more than two quanta on a_u mode and used the 0-0 and 0-2 FC factors to scale the total FC factors obtained with a_u mode excluded. In the second approach, the con-

ventional double harmonic approximation was employed using D_2 geometry of the target state. Likewise, the FC factors for the ${}^2B_{3u}$ state were computed for its equilibrium geometry in the double harmonic approximation. In all cases the FC intensities were convoluted with gaussian functions (FWHM = 0.07 eV) and scaled with Boltzmann weights for $T = 298$ K. The resulting spectra are shown in Fig 5.

Although the 2A_u and ${}^2B_{3u}$ states are separated vertically by 0.38 eV, adiabatically they are almost degenerate with the excitation energies of 2.33 eV and 2.39 eV, respectively. Relaxation from the D_{2h} to D_2 structure lowers the ${}^2A \leftarrow {}^2B_{2g}$ adiabatic excitation energy to 2.22 eV. The absorption profiles calculated assuming either the D_{2h} or D_2 equilibrium geometry are similar. The profiles have a broad structureless shape in the 2.2 - 3.2 eV energy range. The vibrational structure dominated by the ν_5 and ν_6 progressions (Figs. 5A,C) is smeared out by a dense manifold of low frequency transitions associated with deformational out-of-plane motions (Fig. 5B). The intensities of vibronic transitions for the D_2 structure are lower than those at the D_{2h} geometry, which is consistent with the larger geometry changes. Importantly, the shape of the intensity envelope is similar in both cases. We will refer to this bright excited state as 2A_u unless the D_2 2A minimum is mentioned explicitly. The ${}^2B_{3u}$ absorption band is more intense compared to that of 2A_u and exhibits pronounced vibrational structure. Geometry displacements in the ${}^2B_{3u}$ state occur predominantly along the high-frequency normal modes ν_2, ν_3 , which give rise to long vibrational progressions. The 0-0 transition is intense for the ${}^2B_{3u}$ state despite the large geometry relaxation. Possible reason is the frequency lowering of active normal modes in ${}^2B_{3u}$ which is in line with the C-O bond elongation upon excitation. This leads to the frequency decrease by 101 and 313 cm^{-1} for modes ν_2 and ν_3 , respectively. The corresponding vibrational wave functions in the final ${}^2B_{3u}$ state are delocalized and can significantly overlap with the ground-state vibrational wave function of ${}^2B_{2g}$.

Although intensities of the ${}^2B_{3u} \leftarrow {}^2B_{2g}$ vibronic transitions are higher than those of ${}^2A_u \leftarrow {}^2B_{2g}$, the contribution of the latter to the absorption spectrum cannot be neglected because of the high density of 2A_u vibrational states in the interval from 2.2 to 3.2 eV. The ${}^2B_{3u} \leftarrow {}^2B_{2g}$ transition determines the shape of the total excitation envelope and ${}^2A_u \leftarrow {}^2B_{2g}$ introduces additional line smearing. This qualitative feature is independent on the approximation used to evaluate FC of the ${}^2A_u \leftarrow {}^2B_{2g}$ transition. In short, both states can be populated upon 2.3-3 eV excitation, with the absorption to ${}^2B_{3u}$ dominating in the energy range above 2.7 eV.

Determination of a high-resolution gas-phase absorption profiles is problematic owing to

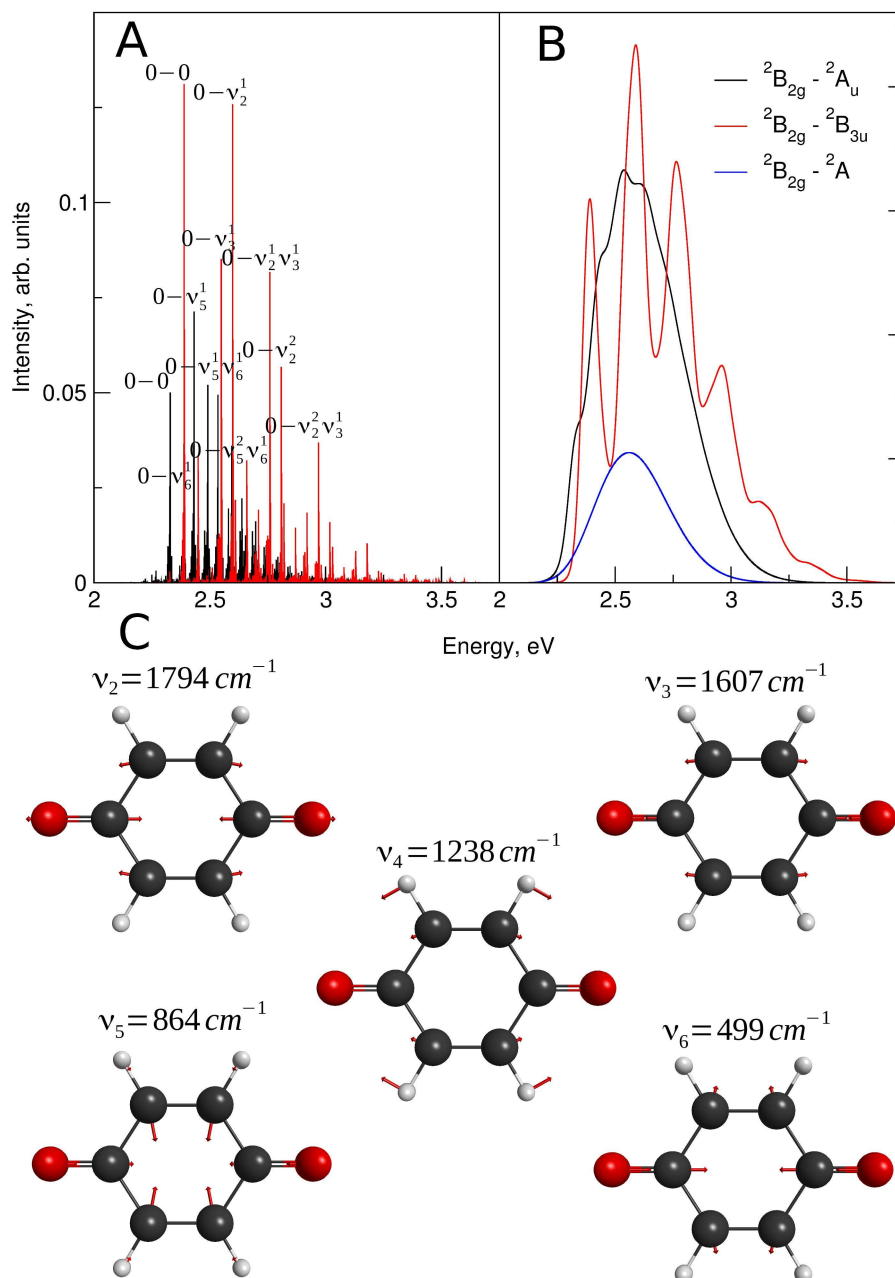


FIG. 5: Vibronic transitions intensities (A) and Gaussian-dressed profiles (B) obtained using the Franck-Condon factors computed within the parallel-normal mode approximation at $T = 298 \text{ K}$. Active normal modes along with vibrational frequencies for ${}^2B_{2g}$ state are also shown (C). The numbering follows Herzberg's convention.

metastable character of the excited states. Yet, absorption spectra have been measured for pBQ \bullet^- radiolytically generated in 2-methyltetrahydrofuran ($T = 77 \text{ K}$) [48] and argon matrices [12, 49]. All the spectra exhibit a vibrationally resolved absorption band centered around 2.9 eV

and an intense band at 3.8 eV. The vibrational features of the low-energy band were identified at 2.7, 2.9 and 3.05 eV [48] with a shoulder at 2.6 eV. Our results indicate that they can be tentatively assigned to the ${}^2B_{3u} \leftarrow {}^2B_{2g}$ vibronic transitions which are red-shifted in our calculation by 0.2-0.3 eV. The shoulder can be possibly explained by the contribution of the lower energy edge of the ${}^2A \leftarrow {}^2B_{2g}$ or ${}^2A_u \leftarrow {}^2B_{2g}$ bands (Fig 5, panel B). The feature at 3.8 eV could be due to $(2) {}^2B_{3u} \leftarrow {}^2B_{2g}$ excitation. The computed vertical energy into $(2) {}^2B_{3u}$ state is 4.25 eV (SI, Section VII). The deviation of the vertical excitation energy from the experimental peak position can be due to (i) matrix effects; and (ii) high relaxation energy of $\text{pBQ}^{\bullet-}$ in the $(2) {}^2B_{3u}$ state causing the red shift of the most intense vibronic transition.

D. Conical Intersections

TABLE II: The energies of minimum energy crossing points (MECP) between the low lying states of $\text{pBQ}^{\bullet-}$ and the two bright excited states (2A_u , ${}^2B_{3u}$). The energies of MECP, eV, are given relative to the equilibrium geometries of the corresponding bright state (2A_u or ${}^2B_{3u}$). CASPT2/CASSCF MECPs energy values reported by Horke et al. [14] are given in parenthesis.

Reference state	2A_u	${}^2B_{3u}$
MECP state		
${}^2B_{1g}$	–	0.13
${}^2B_{2g}$	0.41 (0.47)	0.76 (0.48)
${}^2B_{3g}$	0.13	0.65
2A_u	–	0.11
${}^2B_{2u}$	0.10	1.27
${}^2B_{3u}$	0.20	–

To analyze possible interconversions between bright and dark states we have located relevant MECP points. Multiple low-lying conical intersections are found for both the 2A_u and ${}^2B_{3u}$ states (Table II). Specifically, the ${}^2B_{3u} \times {}^2A_u$ and ${}^2B_{3u} \times {}^2B_{1g}$ MECPs lie 0.11 and 0.13 eV above the ${}^2B_{3u}$ minimum. A series of MECPs with other states was found within 0.65 - 1.27 eV above the ${}^2B_{3u}$ minimum. Similarly, the MECP points of 2A_u with the $n\pi^*$ states are located at 0.1 (${}^2B_{2u}$) and 0.13 eV (${}^2B_{3g}$) relative to the D_{2h} geometry of the 2A_u state (see discussion

in Sec. III B). The located MECPs provide multiple radiationless relaxation channels for the bright excited states of the pBQ \bullet^- anion. The ${}^2A_u \times {}^2B_{3u}$ MECP located just 0.11 eV above the ${}^2B_{3u}$ minimum can facilitate population transfer between the two bright excited states. Multiple low-lying MECPs with the dark excited states of the Feshbach character (${}^2B_{1g}$, ${}^2B_{2u}$, and ${}^2B_{3g}$) can lead to further relaxation to the ground electronic state followed by thermionic emission.

A series of MECPs involving the $\pi\pi^*$ (${}^2A_u, {}^2B_{3u}$), $n\pi^*$ (${}^2B_{2u}, {}^2B_{3g}$), and the ground ${}^2B_{2g}$ state was previously reported by Horke et al. [14]. Overall, the present results are in reasonable agreement with the geometries and energies of Horke et al. [14]. The energy of ${}^2B_{3u} \times {}^2B_{2g}$ MECP is found to be somewhat higher in our calculation (see Table II). We also located a MECP between ${}^2B_{3u}$ and ${}^2B_{1g}$ states that has not been reported in previous computational studies. This MECP lies close to ${}^2B_{3u}$ minimum and can provide additional radiationless relaxation channel along with ${}^2A_u \times {}^2B_{3u}$ crossing.

The role of the MECPs in the photoinduced conversions in pBQ \bullet^- is discussed below in a more detail.

E. Relaxation and electron detachment from the 2A_u and ${}^2B_{3u}$ states

Below we discuss the computed energetics of the excited states in the context of recent spectroscopic studies by Verlet and co-workers [13, 14] with the focus on resonant photodetachment channels that open up at ~ 2.2 eV (Table III). Direct photodetachment channel opens up once the detachment threshold is reached (1.86 eV). As follows from the simulated ${}^2A_u \leftarrow {}^2B_{2g}$ and ${}^2B_{3u} \leftarrow {}^2B_{2g}$ absorption profiles, initial excitation of pBQ \bullet^- at energies below 3.1 eV can populate both bright electronic states (Fig. 5) with ${}^2B_{3u}$ predominantly excited above 2.7 eV. Further evolution of the system may occur via: (a) rapid interconversion between the bright states; (b) autodetachment; (c) non-adiabatic transitions to the $n\pi^*$ states and eventually to the vibrationally excited ${}^2B_{2g}$ state giving rise to thermionic emission peak in the photodetachment spectrum.

Major processes leading to electron emission that open up at particular values of photon energy are listed in Table III. Photoinduced dynamics in pBQ \bullet^- is dominated by the direct photodetachment and autodetachment from the 2A_u state up to 2.39 eV photon energy. Our calculations indicate that conical intersections with dark ${}^2B_{2u}$ and ${}^2B_{1g}$ lie 0.1 eV and 0.13 eV

TABLE III: Main electron ejection channels that open up at different excitation energies. Only new channels that open up at a given energy are listed. Electronic energy differences are presented, adiabatic excitation and detachment energies with zero-point energy correction are given in parenthesis.

Energy, eV	Threshold	Initial absorption	Photoelectron release	Process
1.97 (1.97)	ADE	$^1A_g \leftarrow ^2B_{2g}$	$^1A_g \leftarrow ^2B_{2g}$	direct detachment
2.28 (2.22)	$^2A_u \leftarrow ^2B_{2g}$ AEE	$^2A_u \leftarrow ^2B_{2g}$	$^1A_g \leftarrow ^2A_u$	autodetachment
		$^2A_u \leftarrow ^2B_{2g}$	$^1A_g \leftarrow ^2B_{2g} \leftarrow ^2A_u$	thermionic emission
2.51 (2.39)	$^2B_{3u} \leftarrow ^2B_{2g}$ AEE	$^2B_{3u} \leftarrow ^2B_{2g}$	$^1A_g \leftarrow ^2B_{3u}$	autodetachment
		$^2B_{3u} \leftarrow ^2B_{2g}$	$^1A_g \leftarrow ^2B_{2g} \leftarrow ^2B_{3u}$	thermionic emission
2.64	$^2B_{3u} \times ^2A_u$ MECP	$^2B_{3u} \leftarrow ^2B_{2g}$	$^1A_g \leftarrow ^2A_u \leftarrow ^2B_{3u}$	autodetachment (MECP)
		$^2B_{3u} \leftarrow ^2B_{2g}$	$^1A_g \leftarrow ^2B_{2g} \leftarrow ^2B_{1g} \leftarrow ^2B_{3u}$	thermionic emission
		$^2A_u \leftarrow ^2B_{2g}$	$^1A_g \leftarrow ^2B_{2g} \leftarrow ^2B_{3g} \leftarrow ^2A_u$	thermionic emission
2.86	$^2B_{2g} \times ^2A_u$ MECP	$^2A_u \leftarrow ^2B_{2g}$	$^1A_g \leftarrow ^2B_{2g} \leftarrow ^2A_u$	thermionic emission

above the D_{2h} stationary point (Table II). Therefore, they can facilitate population transfer from the 2A_u state with the following relaxation to the ground state of the anion contributing to the thermionic emission peak. $^2B_{3u}$ becomes accessible at excitation energies above 2.39 eV. The $^2A_u \leftarrow ^2B_{2g}$ and $^2B_{3u} \leftarrow ^2B_{2g}$ absorption cross-sections are similar in magnitude in the energy range of 2.4 - 2.7 eV (Sec. III C) suggesting that both states can participate in photoinduced dynamics. Below we discuss a qualitative photoinduced processes scheme that accounts for the population of both the 2A_u and $^2B_{3u}$ states in the energy range 2.4- 2.7 eV and the observed photoelectron spectrum kinetic energy peak shift from 0.4 to 0.2 eV at 2.7 eV photon energy. Direct detachment at the photon energies of 2.7 eV results in photoelectrons with the kinetic energies ~ 0.7 eV and, thus, does not significantly contribute to the aforementioned feature.

The proposed scheme (Fig. 6) is based on two assumptions. First, the major contribution to the photoelectrons formed upon the resonant photodetachment comes from the 2A_u shape resonance. Autodetachment contribution from $^2B_{3u}$, a Feshbach type resonance, is considered negligible as the lifetime of the Feshbach states is usually higher than that of shape resonances. Second, based on the previous estimates of the lifetime of the 2A_u resonance (51 fs) we assume that the emission occurs vertically once the 2A_u states is reached, i.e., nuclear relaxation occurs on longer time-scale.

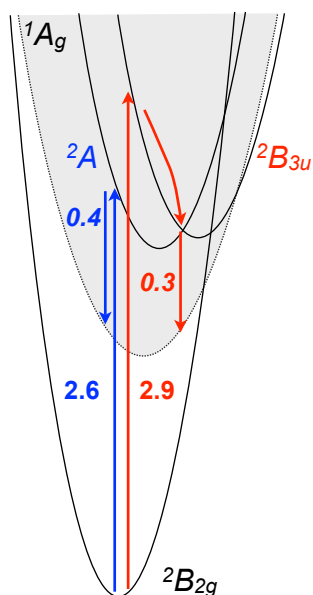


FIG. 6: Autodetachment channels and relevant vertical energy gaps in the case of initial excitation into $2A_u$ state (blue) and $2B_{3u}$ state (red).

Excitation within 2.4–2.7 eV range results in simultaneous population of both bright electronic states, $2A_u$ and $2B_{3u}$. Assuming instantaneous electron ejection and predominant autodetachment from the $2A_u$ state, the resulting kinetic energy of the ejected electrons is ~ 0.4 eV. The estimate is obtained as the vertical energy gap between the $2A_u$ and $1A_g$ states at the equilibrium geometry of the anion (Fig. 7).

Absorption into $2B_{3u}$ dominates above 2.7 eV. $2B_{3u}$ relaxation can occur via electron ejection or via non-adiabatic transitions to $2A_u$, dark excited, or the ground states of the anion. The former process is expected to be slow owing to Feshbach character of the $2B_{3u}$ resonance. Importantly, the dark states located below $2B_{3u}$ are also of Feshbach character. In contrast, non-adiabatic transition to the $2A_u$ state via conical intersection located at 2.6 eV above the ground state minimum (0.1 eV above the $2B_{3u}$ minimum) can lead to fast electron ejection from the $2A_u$ state. Assuming the process occurs instantaneously once the system reaches the $2A_u$ state, e.g. vertical ejection from the MECF point, the resulting kinetic energy of the ejected electron is 0.3 eV, and, thus, is 0.1 eV red shifted w.r.t. direct emission from the $2A_u$ state. This red shift in the photoelectron kinetic energies is consistent with the experimental shift of 0.2 eV once photon energy reaches 2.7 eV. Our theoretical analysis of photodetachment is in qualitative agreement with recent frequency-resolved photoelectron imaging data obtained for excitation energies 2.5 - 3.1 eV [13]. Interestingly, the change of photoelectron energy distribution at 2.7 eV correlates

with abrupt change of PAD anisotropy parameter β_2 from +0.2 to 0.0. This was initially attributed to the new photodetachment channel which opens up at this energy [13]. Note, however, that this observation should be interpreted with caution. Anisotropy changes across resonance states can be due to excitation energy dependent interference of partial waves arising from a single resonant channel and are not necessarily related to additional photodetachment channels [27]. The observed anisotropy disappearance cannot be elucidated based on the energy considerations alone and requires estimates of the relative rates of non-adiabatic transitions as well as more detailed description of autodetachment process.

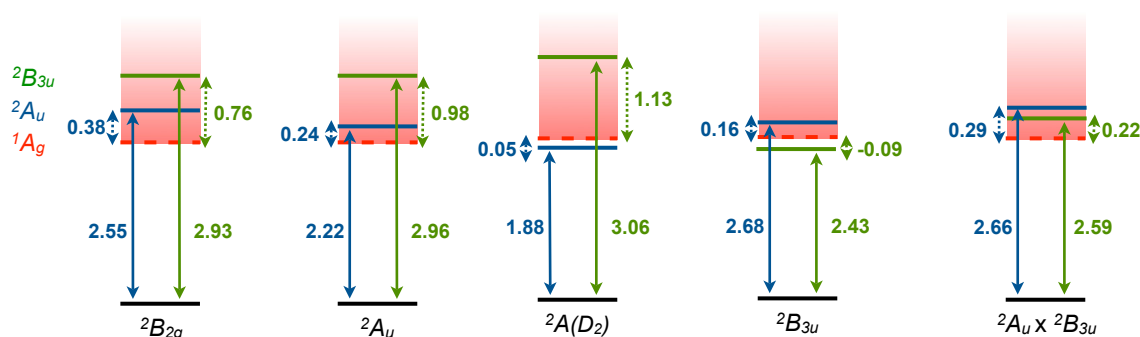


FIG. 7: Relative energies of the ground and the bright excited states of the pBQ \bullet^- anion and ground states of the neutral in several relevant geometries: equilibrium geometry of the ground state of the anion (${}^2B_{2g}$), planar 2A_u configuration (TS), true 2A minimum (D_2 symmetry), the second bright excited state equilibrium geometry (${}^2B_{3u}$), and the MECP point of the ${}^2B_{3u} \times {}^2A_u$ states.

IV. CONCLUSIONS

The results of multireference *ab initio* calculations of pBQ \bullet^- highlight the role of two low-lying bright states, 2A_u and ${}^2B_{3u}$, in photoinduced dynamics of pBQ \bullet^- . The computed Franck-Condon factors of the ${}^2A_u \leftarrow {}^2B_{2g}$ and ${}^2B_{3u} \leftarrow {}^2B_{2g}$ transitions over the energy range 2.4 - 2.7 eV are comparable indicating that the corresponding absorption bands strongly overlap. The equilibrium geometry of the 2A_u state is found to be non-planar (2A state, D_2 symmetry), however, the implications of the geometry twisting on the resulting absorption profile are not significant. The qualitative model accounting for the simultaneous population of the two bright excited state and explaining the experimentally observed shift of the photoelectron kinetic energies peak at 2.7 eV phonon energies is proposed. Overall, non-adiabatic transitions are

expected to play a pivotal role in excited state dynamics of pBQ^{•-} due to a series of conical intersections involving bright excited states in the Franck-Condon region. Complete description of the photodetachment process in pBQ^{•-} requires new theoretical tools capable of treatment non-adiabatic events and electronic decay on equal footing.

-
- [1] H. Nohl and W. Jordan, *Adv. Free Radic. Biol. Med.* **2**, 211 (1986).
 - [2] N. El-Najjar, H. Gali-Muhtasib, R. Ketola, P. Vuorela, A. Urtti, and H. Vuorela, *Photochem. Rev.* **10**, 53370 (2011).
 - [3] W. Hillier and G. Babcock, *Plant Physiol.* **125**, 33 (2001).
 - [4] M. Hohmann-Marriott and R. Blankenship, *Annu. Rev. Plant Biol.* **62**, 525 (2011).
 - [5] A. Millar, J. Whelan, K. Soole, and D. Day, *Annu. Rev. Plant Biol.* **62**, 79 (2011).
 - [6] R. A. Marcus, *Annu. Rev. Phys. Chem.* **15**, 155 (1964).
 - [7] G. L. Closs and J. R. Miller, *Science* **240**, 440 (1988).
 - [8] R. A. Holroyd, *J. Phys. Chem.* **86**, 3541 (1982).
 - [9] A. R. Cook, L. A. Curtiss, and J. R. Miller, *J. Am. Chem. Soc.* **119**, 5729 (1997).
 - [10] R. Holroyd, J. R. Miller, A. R. Cook, and M. Nishikawa, *J. Phys. Chem. B* **118**, 2164 (2014).
 - [11] M. Zamadar, A. R. Cook, A. Lewandowska-Andralojc, R. Holroyd, Y. Jiang, J. Bikalis, and J. R. Miller, *J. Phys. Chem. A* **117**, 8360 (2013).
 - [12] K. Piech, T. Bally, T. Ichino, and J. Stanton, *Phys. Chem. Chem. Phys.* **16**, 2011 (2014).
 - [13] C. W. West, J. N. Bull, E. Antonkov, and J. R. R. Verlet, *J. Phys. Chem. A* **118**, 11346 (2014).
 - [14] D. Horke, Q. Li, L. Blancafort, and J. Verlet, *Nat. Chem.* **5**, 711 (2013).
 - [15] C. D. Cooper, W. T. Naff, and R. N. Compton, *J. Chem. Phys.* **63**, 2752 (1975).
 - [16] M. Allan, *Chem. Phys.* **81**, 235 (1983).
 - [17] P. M. Collins, L. G. Christophorou, E. L. Chaney, and J. G. Carter, *Chem. Phys. Lett.* **4**, 646 (1970).
 - [18] L. G. Christophorou, J. G. Carter, and A. A. Christodoulides, *Chem. Phys. Lett.* **3**, 237 (1969).
 - [19] Q. Fu, J. Yang, and X.-B. Wang, *J. Phys. Chem. A* **115**, 3201 (2011).
 - [20] J. Schiedt and R. Weinkauff, *J. Chem. Phys.* **110**, 304 (1999).
 - [21] N. Moiseyev, *Non-Hermitian quantum mechanics* (Cambridge University Press, 2011).
 - [22] J. Simons and K. D. Jordan, *Chem. Rev.* **87**, 535 (1987).

- [23] J. Simons, *Annu. Rev. Phys. Chem.* **62**, 107 (2011).
- [24] R. Pou-Amérigo, L. Serrano-Andrés, M. Merchán, E. Ortíz, and N. Forsberg, *J. Am. Chem. Soc.* **122**, 6067 (2000).
- [25] Y. Honda, M. Hada, M. Ehara, and H. Nakatsuji, *J. Phys. Chem. A* **106**, 3838 (2002).
- [26] T.-C. Jagau, D. B. Dao, N. S. Holtgrewe, A. I. Krylov, and R. Mabbs, *J. Phys. Chem. Lett.* **6**, 2786 (2015).
- [27] S. Tauro and K. Liu, *J. Phys. B: At. Mol. Opt. Phys.* **41**, 225001 (2008).
- [28] J. N. Bull, C. W. West, and J. R. R. Verlet, *Phys. Chem. Chem. Phys.* (2015).
- [29] W. P. Reinhardt, *Annu. Rev. Phys. Chem.* **33**, 223 (1982).
- [30] K. Bravaya, D. Zuev, E. Epifanovsky, and A. Krylov, *J. Chem. Phys.* **138**, 124106 (2013).
- [31] U. V. Riss and H.-D. Meyer, *J. Phys. B* **26**, 4503 (1993).
- [32] D. Zuev, T.-C. Jagau, K. Bravaya, E. Epifanovsky, Y. Shao, E. Sundstrom, M. Head-Gordon, and A. Krylov, *J. Chem. Phys.* **141**, 024102 (2014).
- [33] T.-C. Jagau, D. Zuev, K. Bravaya, E. Epifanovsky, and A. Krylov, *J. Phys. Chem. Lett.* **5**, 310 (2014).
- [34] A. A. Kunitsa and K. B. Bravaya, *J. Phys. Chem. Lett.* **6**, 10531058 (2015).
- [35] K. Andersson, P.-Å. Malmqvist, B. Roos, A. Sadlej, and K. Wolinski, *J. Phys. Chem.* **94**, 5483 (1990).
- [36] K. Hirao, *Chem. Phys. Lett.* **190**, 374 (1992).
- [37] A. Granovsky, *J. Chem. Phys.* **134**, 214113 (2011).
- [38] S. Gozem, F. Melaccio, R. Lindh, A. Krylov, A. Granovsky, C. Angeli, and M. Olivucci, *J. Chem. Theory Comput.* **9**, 4495 (2013).
- [39] S. Gozem, F. Melaccio, A. Valentini, M. Filatov, M. Huix-Rotllant, N. Ferre, L. Frutos, C. Angeli, A. Krylov, A. Granovsky, et al., *J. Chem. Theory Comput.* (2014), submitted.
- [40] V. Mozhayskiy and A. Krylov, ezSpectrum, <http://iopshell.usc.edu/downloads/>.
- [41] B. G. Levine, J. D. Coe, and T. J. Martnez, *J. Phys. Chem. B* **112**, 405 (2008), ISSN 1520-6106.
- [42] H. A. Witek, Y.-K. Choe, J. P. Finley, and K. Hirao, *J. Comput. Chem.* **23**, 957 (2002).
- [43] A. Granovsky, Firefly version 7.1.G, <http://classic.chem.msu.su/gran/firefly/index.html>.
- [44] M. Schmidt, K. Baldridge, S. E. J.A. Boatz, M. Gordon, S. K. J.H. Jensen, N. Mastunaga, K. Nguyen, T. W. S. Su, M. Dupuis, and J. Montgomery, *J. Comput. Chem.* **14**, 1347 (1993).

- [45] Shao, Y.; Gan, Z.; Epifanovsky, E.; Gilbert, A.T.B.; Wormit, M.; Kussmann, J.; Lange, A.W.; Behn, A.; Deng, J.; Feng, X., et al, *Mol. Phys.* **113**, 184 (2015).
- [46] G. Ghigo, B. Roos, and P.-A. Malmqvist, *Chem. Phys. Lett.* **396**, 142 (2004).
- [47] D. Roca-Sanjuan, M. Merchan, L. Serrano-Andres, and M. Rubio, *J. Chem. Phys.* **129**, 095104 (2008).
- [48] T. Shida, *Electronic Absorption Spectra of Radical Ions* (Elsevier Science Ltd, Amsterdam ; New York, 1989), ISBN 9780444430359.
- [49] J. Gebicki and J. Michl, *J. Phys. Chem.* **92**, 6452 (1988).